Experimental system to detect the electromagnetic response of high-frequency gravitational waves

H. Zheng[1,2] and L. F. Wei[2,*]

[1]*State Key Laboratory of Optoelectronics Materials and Technologies, School of Physics, Sun Yat-sen University, Guangzhou 510275, China*

[2]*Information Quantum Technology Laboratory, School of Information Science and Technology, Southwest Jiaotong University, Chengdu 610031, China*

(Received 21 December 2021; revised 30 August 2022; accepted 11 October 2022; published 3 November 2022)

The mechanical tidal effects of gravitational waves (GWs) in the low- and middle-frequency bands, typically from dozens to hundreds of Hz, have been detected by the LIGO-Virgo-KAGRA ground laser interferometers. To implement the detection of the GWs in the higher-frequency bands (such as the MHz band and the higher ones), predicted by a series of theoretical models in astrophysics and cosmology, we propose here an experimental system to probe their electromagnetic (EM) responses (EMRs). The system mainly consists of a modulated high magnetic field and the weak-light detection techniques (such as single-photon detectors). Physically, when the high-frequency GWs pass through such a modulated high magnetic field, the first-order EMR signals, rather than the second-order ones generated by the inverse Gertsenshtein effects, are induced and can be detected by the current weak-light detection techniques. Interestingly, by considering the influences from the main noises, i.e., the thermal and shot ones, we show that the sensitivity of the proposed system could be utilized to implement the detection of the relic GWs (predicted by the well-known Big Bang model) in the MHz and GHz bands, depending on the frequency of the applied alternating magnetic field. Hopefully, such an experimental system can be built to detect the EMRs of the GWs for testing the relevant gravitational models.

DOI: 10.1103/PhysRevD.106.104003

I. INTRODUCTION

In recent years, a series of astronomical gravitational wave (GW) events have been detected by LIGO-Virgo-KAGRA ground-based laser interferometers [1–6]. These detections verified the existence of the GWs, in the hertz to kilohertz frequency range, generated mainly during the merging processes of the binaries. In fact, detecting the GWs in other frequency bands predicted by a series of theoretical models (see, e.g., in Refs. [7–10]) is also expected. Typically, to detect the lower-frequency GWs beyond the existing laser interferometers, which had been verified by the observations of rotating period damping of the pulsar PSR1913-16 [11,12], many installations including, e.g., the Einstein telescope [13,14], space-based interferometers (such as eLISA- [15], Taiji- [16], and Tianqin [17] plans), atom interferometers [18–20], pulsar timing arrays [21], and cosmic microwave background observations [22,23], etc., have been proposed.

Meanwhile, detecting the GWs in the higher frequencies, typically in 10^6–10^{10} Hz, has also been attracting attention [24,25]. First, a series of cosmic models and high-energy astronomy progresses have predicted the existence of high-frequency GWs (HFGWs), typically, e.g., in Refs. [26–31], etc. Secondly, certain high-energy physics experiments, such as in the high-power laser pulses [32] and Large Hadron Collider (LHC) [33], are also expected to be utilized to generate the HFGWs. Note that all of these models have predicted the GWs with the frequencies being higher than 10^8 Hz. Therefore, a series of proposals and feasible detectors have already been proposed to implement the HFGW detections, typically including the circular waveguide system [34], coupled spherical cavities [35], short- arm interferometers [36,37], microwave and optical cavities [38,39], optically levitated sensors [40], mechanical resonators [41], and the excitation of collective magnon modes [42], etc. [25]. Partially, the electromagnetic (EM) responses (EMR) detection of the HFGW has attracted much attention in recent years (see, e.g., in Refs. [30], etc.).

Originally, the EMR detection of the HFGW is based on the inverse Gertsenshtein effect, i.e., the conversion of the GW into the electromagnet wave (EMW) in a stationary high magnetic field. Unfortunately, detecting the EMR signal of the GW based on the inverse Gertsenshtein effect is very difficult [43–45], as the relevant EMR signal or say the perturbation photon flux (PPF) is very weak (as its density is proportional to the square of the dimensionless amplitude of the detected GW). In order to overcome such a

*lfwei@swjtu.edu.cn

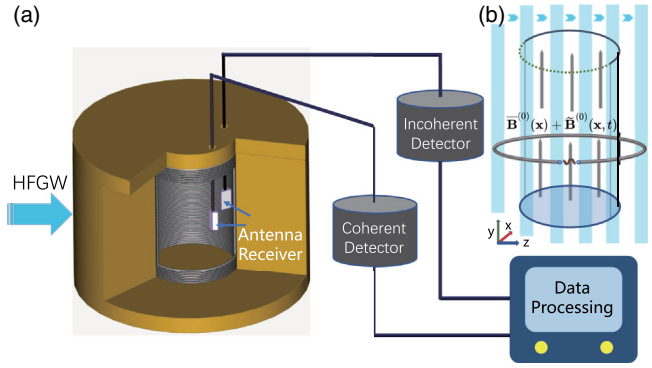

FIG. 1. Experimental system designed to implement the detection of the HFGW. Here, a cylindrical solenoid cavity, whose height is 80 cm, is used to get a high magnetic field, generated by ~21,000-crucible superconducting circle currents. The inner diameter of the solenoid is designed as 30 cm, in which the alternating magnetic field with the frequency of 10^9 Hz can be excited. The antenna receivers are designed to collect the EMR signals of the GW for performing either coherent or incoherent detections. The detection data are then processed to extract the physical parameters of the passing HFGWs.

difficulty, a scheme to amplify the GW-induced PPF by introducing the so-called Gaussian beam resonance technology was proposed in Refs. [46–48], wherein the first-order PPF, rather than the second-order one, could be generated. Recently, we have shown that such a first-order EMR could also be generated if the stationary high magnetic field is modulated by a relatively weak alternating magnetic field [49]. In this paper, we extend our previous work to design an experimental system, whose principle is shown in Fig. 1, for the experimental detections of the HFGWs. The system mainly consists of three parts: a modulated high magnetic field (typically such as 9 T with 0.1 T ac modulated amplitude), the signal-photon detectors (incoherent- and coherent ones), and the detected data processing. The GW-induced EM signals inside the cylindrical cavity can be calculated by numerically solving the Einstein-Maxwell equation in three-dimensional space. Such a signal can be detected by using well-developed weak signal detection techniques. Furthermore, the sensitivity of the proposed detected system can be numerically calibrated by analyzing the noise. The result indicates that the present experimental system could be utilized to implement certain HFGWs, specifically, such as the relic ones, in the GHz band.

The paper is organized as follows. In Sec. II, we demonstrate the basic principle of the detected system, i.e., how the first-order EMRs can be generated when the GWs pass through a cylindrical high magnetic field with the modulating one. In Sec. III, we analyze the characteristics of the signals, typically, e.g., the power, spectral distribution, polarization, wave impedance, etc., and then discuss how to extract the signal from the strong noise background. By analyzing the typical noises, i.e., thermal radiation and shot noises, in Sec. IV, we numerically calibrate the detection sensitivity and show specifically that it could be utilized to implement the detection of certain HFGWs, typically such as the relic ones, in the GHz band. Finally, we summarize our work in Sec. V.

II. MODEL

In order to implement the EMR detections of the GWs, we design an experimental system schematically shown in Fig. 1, wherein a stationary high magnetic field $\bar{\mathbf{B}}^{(0)}(\mathbf{x})$ shown in Fig. 1(a) is generated in a cylindrical solenoid cavity. The height and radius are designed typically as $h = 0.8$ m and $R = 0.15$ m, respectively. The stationary high magnetic field is further modulated by a weak AC magnetic filed with the frequency ω_B and the amplitude $\tilde{\mathbf{B}}_0(\mathbf{x}, t)$, shown, e.g., in Fig. 1(b). The single-photon detectors are located in the cavity to detect the PPFs for later data processing. Certainly, such a system can be realized by the current high magnetic field technologies [50] and weak signal detection technology (coherent and incoherent detection), and thus is feasible.

A. Background fields

The stationary high magnetic field of $\bar{B}_y^{(0)} \sim 10$ T can be obtained by using a circular supercurrent alone, the superconducting solenoid [50]. Indeed, based on Ampere circuital theorem, the stationary high magnetic field at the center of the solenoid reads

$$\bar{B}_y^{(0)} \simeq \mu_0 \frac{NI_{\mathrm{DC}}}{h}, \tag{1}$$

which is towards the positive direction of the y axis. Here, h is the height of the solenoid, N is the number of the superconducting line turns, and I_{DC} is the DC supercurrent. Specifically, if $N = 21000$ and $I_{DC} = 300$ A, then a stationary high magnetic field with $\bar{B}^{(0)} = 9$ T can be obtained [50]. Further, an alternating magnetic field can be generated, in principle, by simply applying an AC current with the frequency of ω_B. Figure 2(a) shows specifically the distribution of a stationary strong magnetic field in the cylindrical cavity, and Fig. 2(b) the alternating one with $\omega_B = 2\pi \times 10^9$ Hz distributed at the point $\mathbf{P} = (0\ \mathrm{m}, 0\ \mathrm{m}, -0.1\ \mathrm{m})$. The basic difference between the present system and the original Gertsenshtein effect configuration is, here an alternating magnetic field is superposed into the original stationary strong magnetic field for generating the first-order (rather than the second-order) EMRs of the passing GWs.

When GWs are absent, the Maxwell equation in flat space-time predicts that an alternating electric field $\tilde{\mathbf{E}}^{(0)}$ determined by

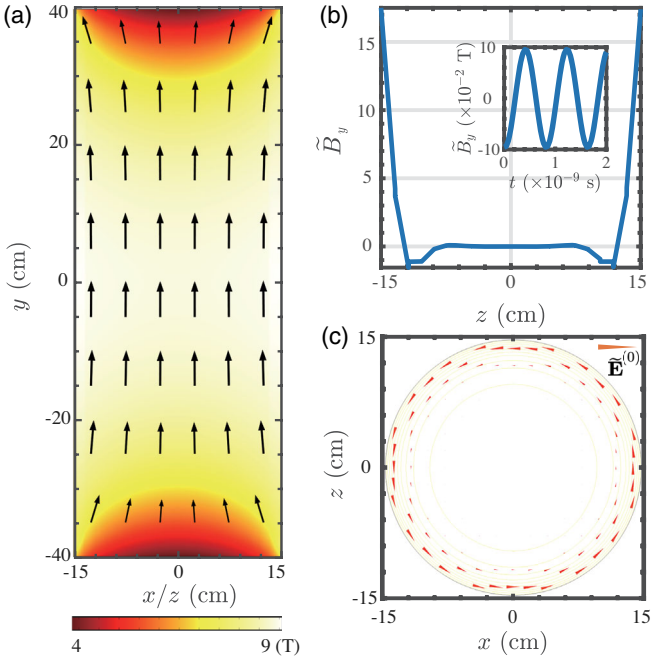

FIG. 2. (a) The distributions of the stationary high magnetic field in the cylindrical solenoid cavity, with $h = 0.8$ m, and $R = 0.15$ m, wherein the arrow refers to the direction of the magnetic field. (b) The alternating magnetic field $\tilde{B}_y^{(0)}$ at the line segment of $x = 0$ m and $y = 0$ m in the cavity is shown, with frequency $\omega_B = 2\pi \times 10^9$ Hz. Inset: alternating magnetic field at point $\mathbf{P} = (0\text{ m}, 0\text{ m}, -0.1\text{ m})$ with $t = [0.2]$ ns. (c) The direction of the zero-order electric field $\tilde{\mathbf{E}}^{(0)}$ generated EM induction at the plane of $y = 0$ m in the cavity by the alternating magnetic field with $\omega_B = 2\pi \times 10^9$ Hz.

$$\nabla \times \tilde{\mathbf{E}}^{(0)}(t) = \frac{\partial \tilde{\mathbf{B}}^{(0)}(t)}{\partial t}, \tag{2}$$

can be generated in the cavity. Its distribution is shown in Fig. 2(c). Therefore, the background magnetic field in cavity is $\mathbf{B}^{(0)} = \bar{\mathbf{B}}^{(0)}(\mathbf{x}) + \tilde{\mathbf{B}}^{(0)}(\mathbf{x}, t)$. As shown in Fig. 2(a), the stationary high magnetic field $\bar{\mathbf{B}}^{(0)}$ in the solenoid cavity is basically evenly distributed, and mainly along the y-axis direction, while, it is seen from Fig. 2(b) that near the cylindrical edge the alternating magnetic field $\tilde{\mathbf{B}}^{(0)} = (0, -\tilde{B}_y^{(0)} \cos(\omega_B t), 0)$, is stronger than those in the center of the cavity. Figure 2(c) shows further how the alternating electric field is distributed on the xz plane. Note that the frequency of the alternating magnetic field ω_B or the phase is adjustable for detecting the HFGWs with different frequencies.

B. Solving the Einstein-Maxwell equation in curved space-time under the GW perturbation

Following Refs. [43,44], the conversion between the GWs and EMWs in a strong static magnetic field can be described by the Einstein-Maxwell equation:

$$\begin{cases} \frac{1}{\sqrt{-g}} \partial_\nu \sqrt{-g} F^{\mu\nu} = 0, \\ \partial_\alpha F_{\beta\gamma} + \partial_\beta F_{\gamma\alpha} + \partial_\gamma F_{\alpha\beta} = 0, \end{cases} \tag{3}$$

where $g = |g_{\alpha\beta}|$ is determinant of the metric $g_{\alpha\beta}$, $F_{\alpha\beta} = \partial_\alpha A_\beta - \partial_\beta A_\alpha$ is the covariant EM fields, A_α is the four-vector potential, and ∂_μ is the partial derivative. The curved space-time, due to the perturbation of the passing GW in transverses-traceless (TT) gauge, is described by the following metric:

$$g_{\alpha\beta} = \eta_{\alpha\beta} + h_{\alpha\beta}(z,t) = \begin{pmatrix} 1 & & & \\ & -1 + h_\oplus(z,t) & h_\otimes(z,t) & \\ & h_\otimes(z,t) & -1 - h_\oplus(z,t) & \\ & & & -1 \end{pmatrix}, \tag{4}$$

with $\eta_{\alpha\beta} = \mathrm{diag}(1, -1, -1, -1)$ and $g = |g_{\alpha\beta}| \simeq |\eta_{\alpha\beta}| = -1$. Note that in the present problem, the choice of TT gauge or proper detector (PD) frame would not lead to any essential difference, at least in the order of the strength of observable effect. The background EM field tensor reads

$$F_{\alpha\beta}^{(0)} = \begin{pmatrix} 0 & 0 & 0 & 0 \\ 0 & 0 & -B_z^{(0)} & B_y^{(0)} \\ 0 & B_z^{(0)} & 0 & -B_x^{(0)} \\ 0 & -B_y^{(0)} & B_x^{(0)} & 0 \end{pmatrix}, \tag{5}$$

where the background EM fields are $\mathbf{B}^{(0)} = \bar{\mathbf{B}}^{(0)}(\mathbf{x}) + \tilde{\mathbf{B}}^{(0)}(\mathbf{x}, t) = (\bar{B}_x^{(0)} + \tilde{B}_x^{(0)}, \bar{B}_y^{(0)} + \tilde{B}_y^{(0)}, \bar{B}_z^{(0)} + \tilde{B}_z^{(0)})$ with $\bar{\mathbf{B}}^{(0)}(\mathbf{x})$ being the stationary high magnetic field, and $\tilde{\mathbf{B}}^{(0)}(\mathbf{x}, t)$ is the alternative magnetic field.

If the GW passes through the cavity, the EM field tensor in the cavity reads

$$F_{\alpha\beta} = F_{\alpha\beta}^{(0)} + F_{\alpha\beta}^{(1)} + F_{\alpha\beta}^{(2)} + \cdots, \tag{6}$$

where the $F_{\alpha\beta}^{(0)}$ is the background magnetic field shown in Eq. (5); $F_{\alpha\beta}^{(1)}$ describes the first-order EMRs related to the dimensionless amplitude of the passing GW. The second-order EMRs $F_{\alpha\beta}^{(2)}$ and the higher-order ones are significantly weak and thus can be ignored. As a consequence, the contravariant form of EMRs under the perturbation of the GWs can be described by the following tensor:

$$F^{\mu\nu} = g^{\mu\alpha}F_{\alpha\beta}g^{\nu\beta} = \begin{pmatrix} 0 & -E_x^{(1)}/c & -E_y^{(1)}/c & -E_z^{(1)}/c \\ E_z^{(1)}/c & 0 & -B_z^{(0)} - B_z^{(1)} & \mathbb{A} \\ E_y^{(1)}/c & B_z^{(0)} + B_z^{(1)} & 0 & -\mathbb{B} \\ E_x^{(1)}/c & -\mathbb{A} & \mathbb{B} & 0 \end{pmatrix}, \tag{7}$$

where $\mathbb{A} = B_y^{(0)}(1+h_\oplus) + B_y^{(1)} - B_x^{(0)}h_\otimes$, $\mathbb{B} = B_x^{(0)}(1-h_\otimes) + B_x^{(1)} - B_y^{(0)}h_\otimes$. Substituting Eqs. (6) and (7) into the Einstein-Maxwell equation (3), the first order of the EMR of the passing GW the electric field $\mathbf{E}^{(1)}$ can be determined by

$$\left(\frac{1}{c^2}\partial_t^2 - \nabla^2\right)\mathbf{E}^{(1)} = \begin{pmatrix} -\partial_t B_y^{(0)}\partial_z h_\oplus - B_y^{(0)}\partial_t\partial_z h_\oplus + \partial_t B_x^{(0)}\partial_z h_\otimes + B_x^{(0)}\partial_t\partial_z h_\otimes \\ -\partial_t B_x^{(0)}\partial_z h_\oplus - B_x^{(0)}\partial_t\partial_z h_\oplus - \partial_t B_y^{(0)}\partial_z h_\otimes - B_y^{(0)}\partial_t\partial_z h_\otimes \\ 0 \end{pmatrix}. \tag{8}$$

In the Appendix, we provide its derivations in detail. A monochrome plane GW propagates along the z-axis direction, with the amplitude $h_\oplus$ and $h_\otimes$. The GW could be described by

$$\begin{cases} h_\oplus(z,t) = h_\oplus \exp\{ik_g(z-ct)\}, \\ h_\otimes(z,t) = ih_\otimes \exp\{ik_g(z-ct)\}, \end{cases} \tag{9}$$

Here, $h_\oplus$ and $h_\otimes$ are the dimensionless amplitude of the GWs with different polarizations. The boundary and initial conditions of the first-order PPFs inside the solenoid cavity are reasonably set as

$$\mathbf{E}^{(1)}|_{y=(-h/2,h/2)} = \mathbf{E}^{(1)}|_{r=R} = 0, \tag{10}$$

and

$$\mathbf{E}^{(1)}|_{t=0} = \partial_t\mathbf{E}^{(1)}|_{t=0} = 0, \tag{11}$$

respectively. Analogously to Eq. (8), the partial differential equations for the magnetic field variables are also given in the Appendix.

C. Electric field distributions of the GW-induced PPF signals

For simplicity and without loss of generality, a GW with the dimensionless amplitude $h_\oplus = h_\otimes = h = 10^{-28}$ is assumed to pass through the solenoid cavity along the z-axis direction. Based on the models mentioned above [26–33], 10^{-28} should be considered as a typical amplitude of the HFGWs in GHz band. Also, the frequency of the applied alternating magnetic field is set as $\omega_B = \omega_g$. For the present cavity geometry, the modes of EM fields in the cavity can be described by three integers (m, n, p) index, where m, n, and p stand for the azimuth, radial, and longitudinal mode indices, respectively. For a cylindrical cavity with the radius and length being 0.15 m and 0.8 m, the frequencies of two typical modes are $\omega_{\mathrm{TE}_{111}} = 2\pi \times 1.234 \times 10^9$ Hz and $\omega_{\mathrm{TM}_{010}} = 2\pi \times 0.766 \times 10^9$ Hz, respectively. By numerically solving Eq. (8), with COMSOL MULTIPHYSICS [51], under the boundary and initial conditions (10), (11), the information of the first-order perturbation electric field caused by the incident GW can be extracted.

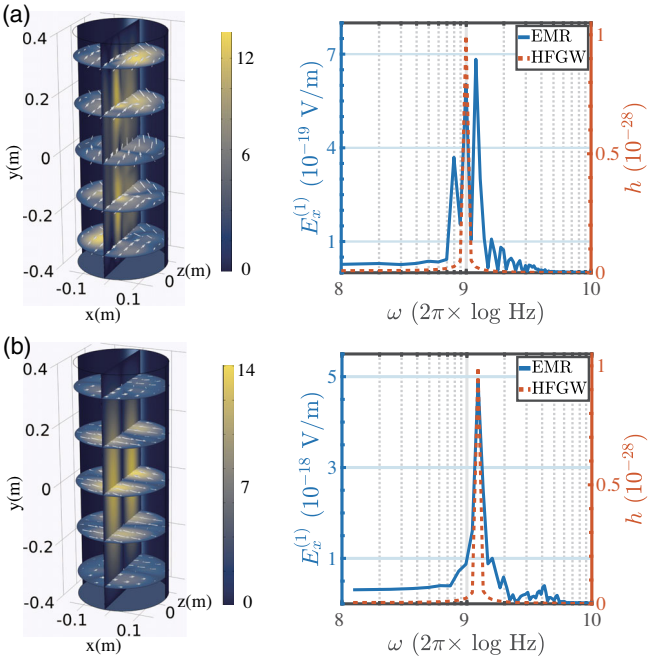

FIG. 3. The first-order perturbation electric field $\mathbf{E}^{(1)}$ distribution in the cavity, with frequency being $\omega = \omega_g$ (left). The spectrum of the $E_x^{(1)}$, at the point $\mathbf{P} = (0\text{ m}, 0\text{ m}, -0.1\text{ m})$ in the cavity (right) generated by the passing HFGWs with $h = 10^{-28}$, $\omega_g = 2\pi \times 10^9$ Hz (a), and $\omega_g = 2\pi \times 1.234 \times 10^9$ Hz (b), respectively. The frequency of the alternating magnetic field is set to be $\omega_B = \omega_g$, $\bar{B}^{(0)} = 9$ T, $\tilde{B}_y^{(0)} = 0.1$ T.

For example, as shown in Fig. 3(a), if the frequency ω_g is near the ones of the TE_{111}- and TM_{010} modes, then both of them can be excited by the first-order PPFs of the GW. As a consequence, three peaks could be observed: one is at $\omega_{TE_{111}}$, one is at $\omega_{TM_{010}}$, and the third one is at $\omega = \omega_g$. Furthermore, as shown in Fig. 3(b), if the frequency of the passing GW equals exactly the frequency of one of the cavity modes, i.e., $\omega = \omega_{TE_{111}}$, then the strongest peak could be observed at this frequency point. Therefore, by observing the signal peaks of the first-order EMRs, the frequency and the relative strength of the passing GW could be determined. By adjusting the frequency of the cylindrical cavity and applying the corresponding near-resonant or resonant alternating magnetic fields, the HFGWs with different frequencies could be searched for. In principle, the proposed system could also be applied to detect the incoherent GWs, which could be practically decomposed as the superposition of a series of coherent ones. In this case, a series of signal peaks could be observed and required to be distinguished by the relevant data analysis. Furthermore, coincidence detection could be implemented for the stochastic GWs. Physically, limited by the geometry size of the cavity, the proposed system is more suitable to implement the EMR detections of the GWs in the GHz and the higher bands. Certainly, the applied alternating magnetic field with the frequency ω_B simultaneously excites the near-resonant and resonant cavity modes, and thus induces the significant background excitations of the cavity modes. These excitations can be treated as background noises, which can be filtered out by using various feasible filtering waves.

III. EMR SIGNAL DETECTIONS

In our previous work [49], we demonstrated that the signal strength is almost independent of the local inertial frame, as it is significantly weak. Hence, the detected first-order PPF signal could be directly determined by the solution to the Einstein-Maxwell equation (8). In this section, the characteristic of the generated signal is investigated.

A. Energy flow density

Theoretically, the EMRs of the passing GWs could be detected by probing the strengths of the GW-induced electric- and magnetic fields. Indeed, the sensitivities of the current metrology on the precise measurements of the electric- and magnetic fields have already reached the levels of $\sim 5 \times 10^{-5}\ \mathrm{V \cdot m^{-1} \cdot Hz^{-1/2}}$ [52] and $\sim 10^{-15}\ \mathrm{T \cdot Hz^{-1/2}}$ [53], respectively. However, one can see from Fig. 3 that the electric field strength of the PPF is just at the level of 10^{-18} V/m. Therefore, the EMR signals are too weak to be detected by their strength measurement. Alternatively, they should be detected by probing their energy responses.

By solving Eq. (8) under the conditions (10), (11), the detectable energy signal of the EMRs can be described by the Poynting vector:

$$\begin{aligned}\mathbf{S} &= \frac{1}{\mu_0}\mathbf{E}(\mathbf{x},t)\times\mathbf{B}(\mathbf{x},t)\\ &= \mathbf{S}^{(0)} + \mathbf{S}^{(1)} + \mathbf{S}'^{(1)} + \mathbf{S}^{(2)},\end{aligned} \tag{12}$$

where

$$\mathbf{S}^{(0)} = \frac{1}{\mu_0}\tilde{\mathbf{E}}^{(0)}(\mathbf{x},t)\times[\bar{\mathbf{B}}^{(0)}(\mathbf{x}) + \tilde{\mathbf{B}}^{(0)}(\mathbf{x},t)], \tag{13}$$

is just related to the background EM field, which can be treated as the zero-order EMR, as it does not carry any GW information. Physically,

$$\mathbf{S}^{(1)} = \frac{1}{\mu_0}\mathbf{E}^{(1)}(\mathbf{x},t)\times[\bar{\mathbf{B}}^{(0)}(\mathbf{x}) + \tilde{\mathbf{B}}^{(0)}(\mathbf{x},t)], \tag{14}$$

and

$$\mathbf{S}'^{(1)} = \frac{1}{\mu_0}\tilde{\mathbf{E}}^{(0)}(\mathbf{x},t)\times\mathbf{B}^{(1)}(\mathbf{x},t), \tag{15}$$

describe energy signals of the first-order EMRs. Obviously, if $\tilde{\mathbf{B}}^{(0)}(\mathbf{x},t)$ is absent, i.e., without the alternating magnetic field, then $\tilde{\mathbf{E}}^{(0)} = 0$, and thus $\mathbf{S}'^{(1)} = 0$. Furthermore, the rapidly oscillating term $\mathbf{E}^{(1)}(\mathbf{x},t)\times\bar{\mathbf{B}}^{(0)}(\mathbf{x})$ vanishes for the average within a limited detected time, and thus, the $\mathbf{S}^{(1)}$ cannot be observed. Therefore, in this case, the strongest detectable effect is related to the second-order EMRs, typically such as

$$\mathbf{S}^{(2)} = \frac{1}{\mu_0}\mathbf{E}^{(1)}(\mathbf{x},t)\times\mathbf{B}^{(1)}(\mathbf{x},t). \tag{16}$$

Certainly, it is significantly weak (as it is related to the square of the relative amplitude of the GW) and thus is hard to be detected.

Alternatively, with the alternating magnetic field $\tilde{\mathbf{B}}^{(0)}(\mathbf{x},t)$, which is assumed to be parallel to the high stationary magnetic field $\bar{\mathbf{B}}^{(0)}$, the EMR signal with the nonzero first-order energy flow densities: $\mathbf{S}^{(1)}$ and $\mathbf{S}'^{(1)}$, could be generated for the detection. The energy detection of a signal is practically a power average within the signal response time. Defining the time average of a detected signal:

$$\langle . \rangle = \frac{1}{\tau}\int_0^\tau dt, \tag{17}$$

with τ being the detected time of the detector, the average energy flow density of the EMRs in the cavity be expressed as

$$\langle\mathbf{S}\rangle = \langle\mathbf{S}^{(0)}\rangle + \langle\mathbf{S}^{(1)}\rangle + \langle\mathbf{S}'^{(1)}\rangle + \langle\mathbf{S}^{(2)}\rangle, \tag{18}$$

with

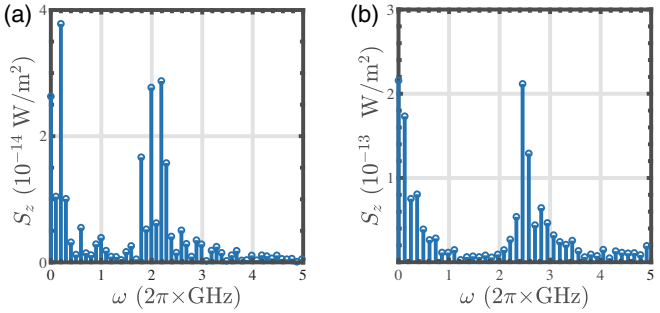

FIG. 4. The spectrum of first-order energy flow intensity $S_z^{(1)}$ [at the point $\mathbf{P} = (0\ \mathrm{m}, 0\ \mathrm{m}, -0.1\ \mathrm{m})$ in the cavity] with the frequency of the passing HFGWs being $\omega_g = 2\pi \times 10^9$ Hz (a), and $\omega_g = 2\pi \times 1.234 \times 10^9$ Hz (b), respectively.

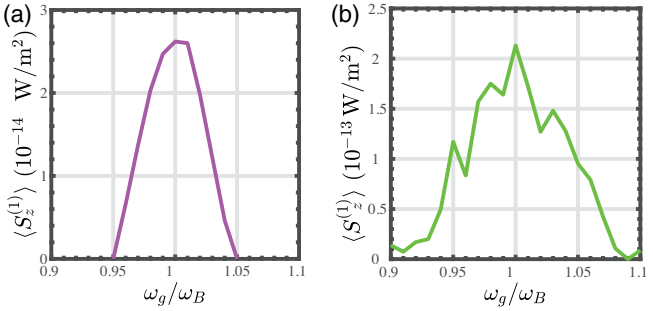

FIG. 5. The averaged energy flow density of the first-order EMR $\langle S_z^{(1)}\rangle$ at the point $\mathbf{P} = (0\ \mathrm{m}, 0\ \mathrm{m}, -0.1\ \mathrm{m})$, in the cavity for the GW with the frequency: $2\pi \times 10^9$ Hz (a), and $2\pi \times 1.234 \times 10^9$ Hz (b), respectively. The frequencies of the alternating magnetic fields in the cavity are set as $\omega_B = 2\pi \times 10^9$ Hz (a), and $\omega_B = 2\pi \times 1.234 \times 10^9$ Hz (b), respectively.

$$\langle \mathbf{S}^{(0)}\rangle = \frac{1}{\mu_0}\langle \tilde{\mathbf{E}}^{(0)}(\mathbf{x},t) \times \tilde{\mathbf{B}}'^{(0)}(\mathbf{x},t)\rangle, \tag{19}$$

being the zero-order EMR signal. It originated from the usual EM induction in the flat space-time and thus can be treated as strong background noise, while the averaged energy flow density of the first-order PPF signals is added by

$$\langle \mathbf{S}^{(1)}\rangle = \frac{1}{\mu_0}\langle \mathbf{E}^{(1)}(\mathbf{x},t) \times \tilde{\mathbf{B}}^{(0)}(\mathbf{x},t)\rangle, \tag{20}$$

and

$$\langle \mathbf{S}'^{(1)}\rangle = \frac{1}{\mu_0}\langle \tilde{\mathbf{E}}^{(0)}(\mathbf{x},t) \times \mathbf{B}^{(1)}(\mathbf{x},t)\rangle. \tag{21}$$

It has been shown that [49] the first-order Poynting vector, either $\langle S^{(1)}\rangle$ or $\langle S'^{(1)}\rangle$, is proportional to the amplitude $\propto h$. Both of them are the first-order EMRs, and they are significantly stronger than those of the second-order ones. Note that in the present configuration, $\tilde{\mathbf{B}}^{(0)}(\mathbf{x},t) = (0, \tilde{B}_y^{(1)}, 0)$ and $E_z^{(1)} = 0$; thus, one of the first-order EMR signals, shown in Eq. (20), can be specifically rewritten as

$$\langle \mathbf{S}^{(1)}\rangle = \left(0, 0, \frac{1}{\mu_0}\langle E_x^{(1)}\tilde{B}_y^{(0)}\rangle\right). \tag{22}$$

Based on the spectrum of $E_x^{(1)}$ shown in Fig. 3 for the scanning frequency ω_B of the applied alternating magnetic field $\tilde{B}_y^{(0)}$, Fig. 4 shows the Fourier transformation $S_z^{(1)}(\omega)$ of the first-order EMR $S_z^{(1)}(t) = E_x^{(1)}(t)\tilde{B}_y^{(0)}/\mu_0$ at a space point $\mathbf{P} = (0\ \mathrm{m}, 0\ \mathrm{m}, -0.1\ \mathrm{m})$ in the cavity. The spectrum shows numerically that for the GWs with the typical frequencies; $\omega = 2\pi \times 10^9$ Hz and $2\pi \times 1.234 \times 10^9$ Hz, a series of first-order EMR signals can be generated in the cavity. Specifically, at the point $\mathbf{P}$ the relatively strong EMR signals are distributed at $\omega = \omega_B - \omega_g$ and $\omega_B + \omega_g$, respectively. The frequency in $S_z^{(1)}(\omega)$ is mainly concentrated around 0 and $2\omega_g$, as the Poynting vector consists of the terms with the frequencies $\omega \pm \omega_B$. This indicates that the EMRs with the frequencies $\omega_S = \omega_B = \omega_g$ and resonant $\omega_S = \omega_B + \omega_g$ are relatively strong, and thus refers to these effects thatcan be called the resonant EMRs of the GW. It means that if the frequency of the applied alternating magnetic field is resonant with the passing GW, then the first-order EMR of the GW is the strongest. This provides the most effective approach to detecting the GWs based on their EMRs. Similarly, the other first-order EMRs of the GW, i.e., $\mathbf{S}'^{(1)}$ can also be analyzed by solving Eq. (A7) to get $\mathbf{B}^{(1)}(\mathbf{x},t)$. As if strength is at the same level as the $\mathbf{S}^{(1)}$, we do not analyze it again. In what follows, we just investigate how to detect the signal with the averaged Poynting vector $\langle \mathbf{S}^{(1)}\rangle$.

Physically, various near-resonant effect can also be detected, although the resonant effect is the strongest. Also, the bandwidth of any detector is usually limited, as the response time of the detection τ in Eq. (17) is definite. For the practical detection, Figs. 5(a) and 5(b) show how $\langle S_z^{(1)}\rangle$ at the point $\mathbf{P} = (0\ \mathrm{m}, 0\ \mathrm{m}, -0.1\ \mathrm{m})$ changes with the frequencies of the passing GWs. Here, the center frequency of the GWs is assumed to be resonant with the modulated frequency of the alternating magnetic field, either $\omega_B = 2\pi \times 10^9$ Hz or $\omega_B = 2\pi \times 1.234 \times 10^9$ Hz, and the response time of the detector is set as $\tau = 10 \times 2\pi/\omega_B$. Certainly, $\langle S_z^{(1)}\rangle$ reaches its maximum value for the resonant case, i.e., $\omega_g = \omega_B$. In Table I, the value of $\langle S_z^{(1)}\rangle$ at the point $\mathbf{P} = (0\ \mathrm{m}, 0\ \mathrm{m}, -0.1\ \mathrm{m})$ in the cavity is listed specifically for the detections of the GWs with the typical frequencies and amplitudes by applying an alternating magnetic field with a given frequency $\omega_B = 2\pi \times 1.234 \times 10^9$ Hz. One can see that the values of $S^{(1)}$ could reach up to 10^{-13} to 10^{-12} W/m^2 for the typical parameters of the HFGWs, which are really detectable by using the current weak signal detection technique. Technologically, the generated first-order EMR signals of

TABLE I. The values of $\langle S_z^{(1)}\rangle$ at the point $\mathbf{P} = (0\ \mathrm{m}, 0\ \mathrm{m}, -0.1\ \mathrm{m})$ in the cavity for the passing GWs with different amplitudes and frequencies. Here, the frequency of the applied alternating magnetic field is set as $\omega_B = 2\pi \times 1.234 \times 10^9$ Hz, $\bar{B}^{(0)} = 9$ T, $\tilde{B}_y^{(0)} = 0.1$ T.

h	ω_g	$\langle S_z^{(1)}\rangle$ (W/m^2)
10^{-27}	0.97 ω_B	1.57×10^{-12}
	1.00 ω_B	2.13×10^{-12}
	1.03 ω_B	1.48×10^{-12}
10^{-28}	0.97 ω_B	1.57×10^{-13}
	1.00 ω_B	2.13×10^{-13}
	1.03 ω_B	1.48×10^{-13}
10^{-29}	0.97 ω_B	1.57×10^{-14}
	1.00 ω_B	2.13×10^{-14}
	1.03 ω_B	1.48×10^{-14}

the GWs could be detected by two methods, coherent- and incoherent detections. Coherent detection is performed by using a local signal to mix the received signal and then treat the mixed one by the usual technique. In fact, coherent detection has been widely used in the EM communication and radar systems. Typically, in the well-known GPS, the detection sensitivity has reached as weak as $10^{-20}\ \mathrm{W}\cdot\mathrm{Hz}^{-1/2}$, which means that $\sim 10^4$ photons per second of the EM signal with the frequency of ~ 1 GHz can be detected with $1-$MHz bandwidth [54]. One can see from Table I that the strength of the generated first-order EMR signal can be really detected, if it really exists. On the other hand, incoherent detection, i.e., the direct detection, has been well developed in recent years by using the single-photon detectors. The generated first-order EMR signals of the passing HFGWs can also be incoherently detected by using the current well-developed single-photon detectors, whose detection sensitivities have arrived at the single-photon energy level [55–60]. The number of the photons in the first-order EMR signal with the energy flow intensity $\langle S_z^{(1)}\rangle = 2.13 \times 10^{-13}\ \mathrm{W/m^2}$ listed in Table I can be simply calculated as $n^{(1)} = \langle S^{(1)}\rangle \Xi/(\hbar\omega_g) \simeq 2.60 \times 10^9\ \mathrm{s}^{-1}$ for $\Xi = 0.01\ \mathrm{m}^2$. Here, Ξ is the area of the photosurface of the applied single-photon detector. It is expected that with the single-photon detection technique, probing the first-order EMRs of the HFGW with the amplitude h being as low as $\sim 10^{-30}$ is also possible, which is likely to cover most of the models mentioned before [26–33].

B. Wave impedance

As motioned above, due to the usual EM induction, the very strong zeroth-order EMRs treated as the background noise are generated in the cavity, the frequency of such a noise could be the same as the ones of the first-order EMRs. This implies that the signal cannot be separated from the noise with the same frequency by using the usual frequency-match filtering-wave technique. Fortunately, the so-called wave-impedance matching technique can be utilized to filter out the noises with the same frequencies [61]. Formally, the wave impedance of an EM wave with frequency ω is defined as the ratio of the transverse components of the electric and magnetic field, i.e.,

$$Z(\omega) = \frac{\mu E_x(\omega)}{B_y(\omega)}, \tag{23}$$

where E_x and B_y are the transverse-electric-magnetic components of a plane wave traveling through a homogeneous medium μ along the z direction. In the present configuration, the wave impedance of the zeroth-order signals in the cavity reads

$$Z_0(\omega_B) = \frac{\mu_0 E_x^{(0)}(\omega_B)}{B_y^{(0)}(\omega_B)} \simeq 377\ \Omega, \tag{24}$$

with μ_0 being the permeability constant in the cavity. However, the wave impedance of the first-order EMR signal with the energy flow density $S_z^{(1)}$ with $\omega_B = \omega_g$ can be expressed alternatively as

$$Z_1(\omega_B) = \frac{\mu_0 E_x^{(1)}(\omega_B)}{B_y^{(0)}(\omega_B)}, \tag{25}$$

which can be specifically calculated as $Z_1(\omega_g) = 5.6 \times 10^{-23}\ \Omega$, for $\omega_g = \omega_B = 2\pi \times 1.234 \times 10^9$ Hz, $\bar{B}_y^{(0)} = 9$ T, $\tilde{B}_y^{(0)} = 0.1$ T, and $\mu_0 = 4\pi \times 10^{-7}\ \mathrm{T}\cdot\mathrm{m}\cdot\mathrm{A}^{-1}$. Apparently, the wave impedance of the first-order EMR signal, carrying the information of the passing GW, is significantly less than that of the zero-order background noise without carrying any information of the GW. Therefore, with the wave-impedance matching technique, the EM signal $\langle \mathbf{S}^{(0)}\rangle$ without any GW information could be effectively filtered out. As a consequence, only the desired signals whose energy flow densities are $\mathbf{S}^{(1)}$ could be conducted into the weak-light detectors for the detections. This implies that by using the wave-impedance matching filtering wave technique to filter out the background noise with the same frequency, detecting the first-order EMR signals of the passing GWs is possible, in principle.

IV. NOISE ANALYSIS AND THE SENSITIVITY DEMARCATION

It is well known that in the laser interferometer system to detect the GWs in the low- and middle-frequency bands, one of the great challenges is to suppress the noises at the same frequency bands. These low-frequency noises should be significantly unimportant for the detection of the HFGWs. As a consequence, only the high-frequency noises influence the detection sensitivity of the proposed experimental system for the detection of the HFGWs.

A. Noise analysis

The strongest noises of the system should be the zero-order EMR signals, which are generated by the usual EM induction without carrying any information about the passing GWs. Therefore, they can be treated as the most important background noises. However, as mentioned before, the physical features of these background noises, typically e.g., the wave impedance, are very different from those of the first-order EMR signals. Therefore, these background noises, together with the other external high-frequency EM noises (described also by the usual Maxwell equation in flat space-time), can be effectively filtered out by applying the relevant wave-impedance matching filtering techniques. As a consequence, the main noises in the present experimental system are the thermal noises and the shot noises in the same frequency band.

Physically, thermal radiation noises exist in any experimental system. As a consequence, they must influence measurement accuracy. In the proposed experimental system, the high magnetic field is practically built by the superconducting lines. Thus, the system can practically work in different temperatures, typically such as in the 5, 0.5, and even 0.05 K, respectively. In fact, the thermal noises cannot be neglected, as the thermal energy unit $K_{\mathrm{B}}T$ at ultralow temperature is almost the same as the energy of the single photon $\hbar\omega_g$ in the microwave band. Specifically, the power of the thermal noises can be expressed as [62]

$$P_{\mathrm{Therm}}=\frac{\hbar\omega^3\Delta\omega}{2\pi c^2}\frac{1}{e^{\hbar\omega/(K_{\mathrm{B}}T)}-1}, \tag{26}$$

with ω being the signal frequency, $\Delta\omega$ is response bandwidth of the detector, K_{B} is the Boltzmann constant, and T is the working temperature of the system.

Secondly, the shot noises play an important role in all the weak signal detection systems. The detection of the significantly weak EM signals is equivalent to count the number n of the detected photons, which obey the usual Poisson distribution:

$$p(n)=\frac{\bar{n}^n\exp(-\bar{n})}{n!}, \tag{27}$$

where $\bar{n}$ is the averaged number of the photons. For a signal with frequency ω and power P_{S}, the number of the photons per second is $n=P_{\mathrm{S}}\Xi/\hbar\omega$, where the standard deviation of the photon statistics could be roughly expressed as $\sqrt{\bar{n}\tau}$. Consequently, the power of the shot noises can be expressed as

$$P_{\mathrm{Shot}}=\sqrt{\frac{P_{\mathrm{S}}\hbar\omega}{\Xi\tau}}. \tag{28}$$

These noises limit the sensitivity of the proposed experimental system for the EMR detection of the HFGWs.

B. Sensitivity

Usually, the sensitivity of the detector is defined as its minimum detectable power. For the present system, the detection sensitivity refers to the minimum amplitude of the detectable GWs. Physically, noises determine the sensitivity of the detector, and thus the equivalent noise power (NEP) is defined as the noise power when the signal-to-noise ratio equals to 1, i.e., if $\mathrm{SNR}=P_{\mathrm{S}}/P_{\mathrm{N}}=1$, we have $\mathrm{NEP}=P_{\mathrm{N}}$. Above, P_{S} is the power of the signal and P_{N} is the power of the noises. In the present experimental system, the power of the noises is $P_{\mathrm{N}}=P_{\mathrm{Therm}}+P_{\mathrm{Shot}}$, and the power of the signal, i.e., the first-order EMRs, reads $P_{\mathrm{S}}=\langle S_z^{(1)}\rangle\Xi$, which it is proportional to the amplitude of the passing GW. Therefore, the minimum detectable amplitude of the HFGW can be defined as h^{min}, which means that the minimum detectable signal power per square meter is

$$\mathrm{NEP}=h^{\mathrm{min}}\mathbb{S}, \tag{29}$$

with $\mathbb{S}=\langle S_z^{(1)}\rangle/h$. Therefore, the minimum detectable amplitude h^{min} of the HFGWs, i.e., the sensitivity of the system, can be determined by

$$h^{\mathrm{min}}\mathbb{S}-\sqrt{\frac{\hbar\omega}{\Xi\tau}}\cdot\sqrt{h^{\mathrm{min}}\mathbb{S}}-P_{\mathrm{Therm}}=0. \tag{30}$$

Therefore,

$$h^{\mathrm{min}}=\frac{1}{2\mathbb{S}}\left[\frac{\hbar\omega}{\Xi\tau}+2P_{\mathrm{Therm}}+\sqrt{\left(\frac{\hbar\omega}{\Xi\tau}\right)^2+4\frac{\hbar\omega}{\Xi\tau}P_{\mathrm{Therm}}}\right]. \tag{31}$$

In Fig. 6, we show the sensitivity of the designed system to resonantly detect the first-order EMRs of the passing GWs with the frequencies being $\omega_g=2\pi\times10^9$ Hz and $\omega_g=2\pi\times1.234\times10^9$ Hz, respectively. The location of the single-photon detector with the area $\Xi=0.01\ \mathrm{m}^2$ is assumed to be put at the point $\mathbf{P}=(0\ \mathrm{m},0\ \mathrm{m},-0.1\ \mathrm{m})$ in the cavity, and the response time of the detector is set as $\tau=10\times2\pi/\omega_g$.

Of course, the modulated frequency ω_B of the alternating magnetic field can be adjusted, if the GWs with different center frequencies are expected to be probed. Figure 6 implies that for a given frequency of the applied alternating magnetic field ω_B, the first-order EM responses of the passing GWs with the frequency $\omega_g=\omega_B$ are the strongest, although the response of the GWs with the frequency near such a center frequency is also generated. It is seen clearly that the sensitive regime of the system is located really near the centered frequency point. The minimum detectable amplitude of the passing GW could be less than 10^{-30}, if the stationary high magnetic field is modulated by an

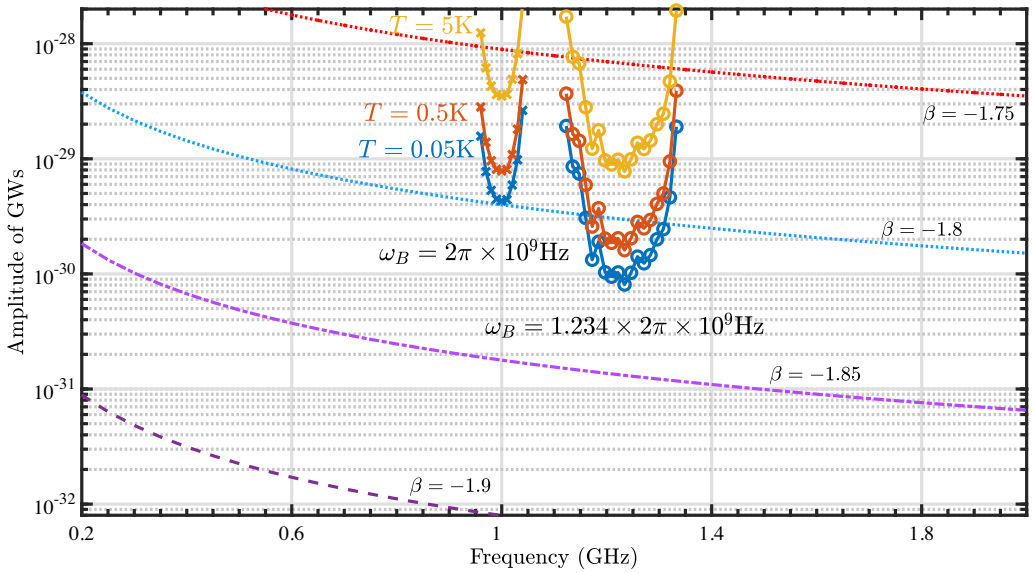

FIG. 6. Sensitivity of the designed experimental system for the detection of the GWs with the centered frequencies being $2\pi \times 10^9$ Hz and $2\pi \times 1.234 \times 10^9$ Hz, respectively. Here, the modulated alternating magnetic field is set as $\omega_B = 2\pi \times 10^9$ Hz or $\omega_B = 2\pi \times 1.234 \times 10^9$ Hz and $\bar{B}_y^{(0)} = 9$ T, $\tilde{B}_y^{(0)} = 0.1$ T. The dashed lines represent the frequency-dependent amplitudes of the relic GWs with different β parameters [8].

alternating magnetic field with the frequency as the GW, i.e., $\omega_B = \omega_g = 1.234 \times 10^9$ Hz. It is nothing but the frequency of one of the standing modes in the cavity. Naturally, the higher stationary high magnetic field and the stronger modulated alternating magnetic field lead to the higher sensitivity. Still, the system could be utilized to detect the GWs with the higher frequencies by using the corresponding alternating magnetic field to excite the relevant standing-wave modes in the cavity, resonantly.

C. The possibility to detect the high-frequency relic GWs in microwave band

Based on the above sensitive demarcation, we now discuss if the designed experimental system could be utilized to implement the detections of the typical HFGWs, i.e., the relic GWs predicted by the Big Bang Theory (see, e.g., [7–10,28]). It is well known that the band of the relic GWs is very wide, i.e., from 10^{-18} to 10^{10} Hz [63]. In fact, the targets of the BICEP-II- [22] and Ali programs [23] are to detect the relic GWs in the significantly low-frequency band. Differently, our aim is to detect the relic GWs in the high-frequency band, i.e., its frequency is near 10^9 Hz. Basically, the amplitude of relic GW can be expressed as [8]

$$h(\omega) = 0.37 \times 10^{-5} \left(\frac{\omega}{\omega_H}\right)^{1+\beta-\beta_s} \cdot \left(\frac{\omega_s}{\omega_H}\right)^{\beta_s} \cdot \frac{\omega_H}{\omega_2}, \qquad (32)$$

in the higher-frequency band, i.e., from 10^5 to 10^{10} Hz. Above, $\omega_H = 4\pi \times 10^{-18}$ Hz, $\omega_2 = 2.36\pi \times 10^{-16}$ Hz, $\omega_s = 2\pi \times 10^8$ Hz, $\omega_1 = 6\pi \times 10^{10}$ Hz, and $\beta_s = 0.598$. Above, β is an important parameter to describe the expansion index of the cosmic inflation. Given different models (see, e.g., [8,64]) predict the different values of this parameter, we believe that these models can be experimentally tested by using the present system. Specifically, one can see from Fig. 6 that the experimental system, with $\bar{B}_0 = 9$ T, $\tilde{B}_y^{(1)} = 0.1$ T, $\omega_B = 2\pi \times 10^9$ Hz or $\omega_B = 2\pi \times 1.234 \times 10^9$ Hz designed in this work can be utilized to implement the detections of the relic GWs with the frequencies near $2\pi \times 10^9$ Hz or $2\pi \times 1.234 \times 10^9$ Hz. If the desired first-order EMR signals can be detected, then the β paramter should be larger than -1.8 [64]. Therefore, these detections are useful to determine the upper-limit value of the β parameter in the relevant theoretical models. Finally, by enhancing the frequency of the modulated high magnetic field, detections of the GWs with the higher frequencies are also possible.

V. CONCLUSIONS AND DISCUSSION

As the complementation of various installations to detect the GWs in low- and middle-frequency bands, in this paper, we have designed an experimental system to detect the GWs in the microwave frequency band. The basic idea is to detect the resonant first-order EMRs of the HFGWs passing through a stationary magnetic field system modulated by a resonant alternating magnetic field. This detection principle and method are basically different from the well-known laser interferometers for detecting the mechanical tidal effects of the GWs in the low- and middle-frequency bands.

In the proposed system, an alternating magnetic field is applied to modulate the stationary high magnetic field for amplifying the undetectable second-order Gertsenshtein effects to become the detectable first-order EMRs. Basically, such an experimental system is achievable with the current high magnetic field and single-photon detection techniques. Furthermore, based on the noise analysis of the system, we argued that the sensitivity of the designed experimental system meets the requirement of the detection of the relic GWs in the microwave band. At least, the proposed system could be utilized to determine the upper limits of certain important parameters in the relevant theoretical models on the HFGWs.

Certainly, the experimental implementation of the proposed system is still a great technical challenge. For example, limited by the size of the artificial high magnetic field system, the proposed system cannot be used to implement the detection of the GWs with lower frequencies, i.e., less than 10^8 Hz. Also, for the current technique, the amplitude of the applied high-frequency alternating magnetic field cannot be sufficiently large. This limits the strength of the generated first-order EMRs of the passing GWs for the detections. Anyway, we argued that the detections of certain HFGWs with the proposed experimental system are feasible. At least, these detections are useful to determine the upper limits of the physical parameters in the relevant theoretical models.

ACKNOWLEDGMENTS

This work is partially supported by the National Natural Science Foundation of China, Grant No. 11974290. We thank Professor Q. Q. Jiang, Professor F. Y. Li, Professor J. Li, Professor Y. Zhao, and Professor L. S. Yan for the useful discussions and Dr. M. Hussain for correcting our English.

APPENDIX: MAXWELL EQUATIONS FOR THE EM FIELD IN THE CAVITY PERTURBATED BY A GW

We assume that a monochromatic GW passes though the cavity and toward the z–axis direction. Its amplitude is h and frequency is ω_g. Now, with the alternating magnetic field, the EM tensor in the solenoid cavity is described by Eq. (5). After the perturbation of the passing GW, the EM tensor reads

$$F_{\alpha\beta} \simeq F^{(0)}_{\alpha\beta} + F^{(1)}_{\alpha\beta} = \begin{pmatrix} 0 & E^1_x/c & E^{(1)}_y/c & E^{(1)}_z/c \\ -E^{(1)}_x/c & 0 & -\mathbb{Z} & \mathbb{Y} \\ -E^{(1)}_y/c & \mathbb{Z} & 0 & -\mathbb{X} \\ -E^{(1)}_z/c & -\mathbb{Y} & \mathbb{X} & 0 \end{pmatrix}, \quad \text{(A1)}$$

under the driving of the GW. Here, the $F^{(1)}_{\alpha\beta}$ represents the first-order EMRs of the passing HFGWs, and

$$\mathbb{X} = B^{(0)}_x + B^{(1)}_x, \quad \mathbb{Y} = B^{(0)}_y + B^{(1)}_y, \quad \mathbb{Z} = B^{(0)}_z + B^{(1)}_z.$$

With the space-time metric (4), the contravariant form of the above EM field tensor $F^{\mu\nu} = g^{\mu\alpha}F_{\alpha\beta}g^{\nu\beta}$ takes the form shown in Eq. (7), by neglecting the second-order and higher-order responses.

In general, the amplitude of GW is very small; therefore, the determinant of the metric can be approximated as $g \backsimeq -1$. Thus, the first Eq. (3) becomes

$$\partial_\nu F^{\mu\nu} = 0. \quad \text{(A2)}$$

Substituting Eq. (7) into Eq. (A2), we have

$$\nabla \cdot \mathbf{E}^{(1)} = 0, \quad \text{(A3)}$$

and

$$\frac{1}{c^2}\partial_t \mathbf{E}^{(1)} - \nabla \times \mathbf{B}^{(1)} = \begin{pmatrix} B^{(0)}_y \partial_z h_\otimes - B^{(0)}_y \partial_z h_\oplus \\ -B^{(0)}_x \partial_z h_\oplus - B^{(0)}_y \partial_z h_\otimes \\ B^{(0)}_y \partial_x h_\oplus + B^{(0)}_x \partial_y h_\oplus - B^{(0)}_x \partial_x h_\otimes + B^{(0)}_y \partial_y h_\otimes \end{pmatrix}. \quad \text{(A4)}$$

Also substitute Eq. (A1) into the second one of Eq. (3); similarly, we have

$$\nabla \cdot \mathbf{B}^{(1)} = 0, \quad \text{(A5)}$$

and

$$\frac{1}{c^2}\partial_t \mathbf{B}^{(1)} - \nabla \times \mathbf{E}^{(1)} = 0. \quad \text{(A6)}$$

Above, the noise term $\partial_t \mathbf{B}^{(0)}$ is neglected. Meanwhile, $\partial_i \mathbf{B}^{(0)} = 0$, where $i = x, y, x$, as $\mathbf{B}^{(0)}$ is the stationary magnetic field in the cavity.

With Eqs. (A3)–(A6), we get Eq. (8) and

$$\left(\frac{1}{c^2}\partial_t^2 - \nabla^2\right)\mathbf{B}^{(1)} = \begin{pmatrix} -B^{(0)}_x \partial_z^2 h_\oplus - B^{(0)}_y \partial_z^2 h_\otimes \\ -B^{(0)}_x \partial_z^2 h_\otimes - B^{(0)}_y \partial_z^2 h_\oplus \\ 0 \end{pmatrix}. \quad \text{(A7)}$$

By solving Eq. (A7), the magnetic components $\mathbf{B}^{(1)}$ of the first-order EMRs, induced by the GW perturbations, can be obtained, similarly.

[1] B. P. Abbott *et al.* (LIGO Scientific and Virgo Collaborations), Observation of Gravitational Waves from a Binary Black Hole Merger, Phys. Rev. Lett. **116**, 061102 (2016).

[2] B. P. Abbott *et al.* (LIGO Scientific and Virgo Collaborations), GW151226: Observation of Gravitational Waves from a 22-Solar-Mass Binary Black Hole Coalescence, Phys. Rev. Lett. **116**, 241103 (2016).

[3] B. P. Abbott *et al.* (LIGO Scientific and Virgo Collaboration), GW170104: Observation of a 50-Solar-Mass Binary Black Hole Coalescence at Redshift 0.2, Phys. Rev. Lett. **118**, 221101 (2017).

[4] B. P. Abbott *et al.* (LIGO Scientific and Virgo Collaborations), GW170814: A Three-Detector Observation of Gravitational Waves from a Binary Black Hole Coalescence, Phys. Rev. Lett. **119**, 141101 (2017).

[5] B. P. Abbott *et al.* (LIGO Scientific and Virgo Collaborations), GW170817: Observation of Gravitational Waves from a Binary Neutron Star Inspiral, Phys. Rev. Lett. **119**, 161101 (2017).

[6] B. P. Abbott *et al.* (LIGO Scientific and Virgo Collaborations), GW170608: Observation of a 19 solar-mass binary black hole coalescence, Astrophys. J. Lett. **851**, L35 (2017).

[7] A. H. Guth, Inflationary universe: A possible solution to the horizon and flatness problems, Phys. Rev. D **23**, 347 (1981).

[8] Y. Zhang, Y. Yuan, W. Zhao, and Y.-T. Chen, Relic gravitational waves in the accelerating universe, Classical Quantum Gravity **22**, 1383 (2005).

[9] M. L. Tong and Y. Zhang, Relic gravitational waves with a running spectral index and its constraints at high frequencies, Phys. Rev. D **80**, 084022 (2009).

[10] B. P. Abbott *et al.* (LIGO Scientific and Virgo Collaborations), An upper limit on the stochastic gravitational-wave background of cosmological origin, Nature (London) **460**, 990 (2009).

[11] R. A. Hulse, The discovery of the binary pulsar, Rev. Mod. Phys. **66**, 699 (1994).

[12] J. H. Taylor, Binary pulsars and relativistic gravity, Rev. Mod. Phys. **66**, 711 (1994).

[13] M. Punturo *et al.*, The Einstein telescope: A third-generation gravitational wave observatory, Classical Quantum Gravity **27**, 194002 (2010).

[14] K. Craig, J. Steinlechner, P. G. Murray, A. S. Bell, R. Birney, K. Haughian, J. Hough, I. MacLaren, S. Penn, S. Reid, R. Robie, S. Rowan, and I. W. Martin, Mirror Coating Solution for the Cryogenic Einstein Telescope, Phys. Rev. Lett. **122**, 231102 (2019).

[15] A. Klein, E. Barausse, A. Sesana, A. Petiteau, E. Berti, S. Babak, J. Gair, S. Aoudia, I. Hinder, F. Ohme, and B. Wardell, Science with the space-based interferometer eLISA: Supermassive black hole binaries, Phys. Rev. D **93**, 024003 (2016).

[16] G. Wang, W.-T. Ni, W.-B. Han, S.-C. Yang, and X.-Y. Zhong, Numerical simulation of sky localization for LISA-TAIJI joint observation, Phys. Rev. D **102**, 024089 (2020).

[17] S.-J. Huang, Y.-M. Hu, V. Korol, P.-C. Li, Z.-C. Liang, Y. Lu, H.-T. Wang, S. Yu, and J. Mei, Science with the TianQin observatory: Preliminary results on galactic double white dwarf binaries, Phys. Rev. D **102**, 063021 (2020).

[18] L. Badurina *et al.*, AION: An atom interferometer observatory and network, J. Cosmol. Astropart. Phys. 05 (2020) 011.

[19] M. Abe *et al.*, Matter-wave atomic gradiometer interferometric sensor (MAGIS-100), Quantum Sci. Technol. **6**, 044003 (2021).

[20] Y. A. El-Neaj *et al.*, AEDGE: Atomic experiment for dark matter and gravity exploration in space, Eur. Phys. J. Quantum Technol. **7**, 6 (2020).

[21] Z. Arzoumanian *et al.*, The NANOGrav 12.5 yr data set: Search for an isotropic stochastic gravitational-wave background, Astrophys. J. Lett. **905**, L34 (2020).

[22] K. M. Smith, C. Dvorkin, L. Boyle, N. Turok, M. Halpern, G. Hinshaw, and B. Gold, Quantifying the BICEP2-Planck Tension over Gravitational Waves, Phys. Rev. Lett. **113**, 031301 (2014).

[23] H. Li, S.-Y. Li, Y. Liu, Y.-P. Li, Y. Cai, M. Li, G.-B. Zhao, C.-Z. Liu, Z.-W. Li, H. Xu, D. Wu, Y.-J. Zhang, Z.-H. Fan, Y.-Q. Yao, C.-L. Kuo, F.-J. Lu, and X. Zhang, Probing primordial gravitational waves: Ali CMB Polarization Telescope, Natl. Sci. Rev. **6**, 145 (2018).

[24] N. Aggarwal *et al.*, Challenges and opportunities of gravitational-wave searches at MHz to GHz frequencies, Living Rev. Relativity **24**, 4 (2021).

[25] A. Berlin, D. Blas, R. T. D'Agnolo, S. A. R. Ellis, R. Harnik, Y. Kahn, and J. Schütte-Engel, Detecting high-frequency gravitational waves with microwave cavities, Phys. Rev. D **105**, 116011 (2022).

[26] M. Servin and G. Brodin, Resonant interaction between gravitational waves, electromagnetic waves, and plasma flows, Phys. Rev. D **68**, 044017 (2003).

[27] G. S. Bisnovatyi-Kogan and V. N. Rudenko, Very high frequency gravitational wave background in the universe, Classical Quantum Gravity **21**, 3347 (2004).

[28] M. Giovannini, Production and detection of relic gravitons in quintessential inflationary models, Phys. Rev. D **60**, 123511 (1999).

[29] S. S. Seahra, C. Clarkson, and R. Maartens, Detecting Extra Dimensions with Gravity-Wave Spectroscopy: The Black-String Brane World, Phys. Rev. Lett. **94**, 121302 (2005).

[30] N. Herman, A. Fűzfa, L. Lehoucq, and S. Clesse, Detecting planetary-mass primordial black holes with resonant electromagnetic gravitational-wave detectors, Phys. Rev. D **104**, 023524 (2021).

[31] J. Liu, Z.-K. Guo, R.-G. Cai, and G. Shiu, Gravitational Waves from Oscillons with Cuspy Potentials, Phys. Rev. Lett. **120**, 031301 (2018).

[32] H. Kadlecová, O. Klimo, S. Weber, and G. Korn, Gravitational wave generation by interaction of high power lasers with matter using shock waves, Eur. Phys. J. D **71**, 89 (2017).

[33] X.-G. Wu and Z.-Y. Fang, Revisiting the real graviton effects at CERN LHC within the quantum gravity theory with large extra dimensions, Phys. Rev. D **78**, 094002 (2008).

[34] A. M. Cruise, An electromagnetic detector for very-high-frequency gravitational waves, Classical Quantum Gravity **17**, 2525 (2000).

[35] R. Ballantini, P. Bernard, E. Chiaveri, A. Chincarini, G. Gemme, R. Losito, R. Parodi, and E. Picasso, A detector of

high frequency gravitational waves based on coupled microwave cavities, Classical Quantum Gravity **20**, 3505 (2003).

[36] T. Akutsu, S. Kawamura, A. Nishizawa, K. Arai, K. Yamamoto, D. Tatsumi, S. Nagano, E. Nishida, T. Chiba, R. Takahashi, N. Sugiyama, M. Fukushima, T. Yamazaki, and M.-K. Fujimoto, Search for a Stochastic Background of 100-MHz Gravitational Waves with Laser Interferometers, Phys. Rev. Lett. **101**, 101101 (2008).

[37] A. Nishizawa, S. Kawamura, T. Akutsu, K. Arai, K. Yamamoto, D. Tatsumi, E. Nishida, M.-a. Sakagami, T. Chiba, R. Takahashi, and N. Sugiyama, Laser-interferometric detectors for gravitational wave backgrounds at 100 MHz: Detector design and sensitivity, Phys. Rev. D **77**, 022002 (2008).

[38] A. Cruise and R. Ingley, A prototype gravitational wave detector for 100 MHz, Classical Quantum Gravity **23**, 6185 (2006).

[39] A. Arvanitaki and A. A. Geraci, Detecting High-Frequency Gravitational Waves with Optically Levitated Sensors, Phys. Rev. Lett. **110**, 071105 (2013).

[40] N. Aggarwal, G. P. Winstone, M. Teo, M. Baryakhtar, S. L. Larson, V. Kalogera, and A. A. Geraci, Searching for New Physics with a Levitated-Sensor-Based Gravitational-Wave Detector, Phys. Rev. Lett. **128**, 111101 (2022).

[41] M. Goryachev and M. E. Tobar, Gravitational wave detection with high frequency phonon trapping acoustic cavities, Phys. Rev. D **90**, 102005 (2014).

[42] A. Ito and J. Soda, A formalism for magnon gravitational wave detectors, Eur. Phys. J. D **80**, 545 (2020).

[43] M. E. Gertsenshtein, Wave resonance of light and gravitational waves, Sov. Phys. JETP Lett. **14**, 84 (1962).

[44] Y. B. Zel'dovich, Electromagnetic and gravitational waves in a stationary magnetic field, Sov. Phys. JETP Lett. **65**, 1311 (1973).

[45] A. Ejlli, D. Ejlli, A. M. Cruise, G. Pisano, and H. Grote, Upper limits on the amplitude of ultra-high-frequency gravitational waves from graviton to photon conversion, Eur. Phys. J. C **79**, 1032 (2019).

[46] F.-Y. Li, M.-X. Tang, and D.-P. Shi, Electromagnetic response of a gaussian beam to high-frequency relic gravitational waves in quintessential inflationary models, Phys. Rev. D **67**, 104008 (2003).

[47] F. Li, N. Yang, Z. Fang, R. M. L. Baker, G. V. Stephenson, and H. Wen, Signal photon flux and background noise in a coupling electromagnetic detecting system for high-frequency gravitational waves, Phys. Rev. D **80**, 064013 (2009).

[48] F. Li, H. Wen, Z. Fang, L. Wei, Y. Wang, and M. Zhang, Quasi-b-mode generated by high-frequency gravitational waves and corresponding perturbative photon fluxes, Nucl. Phys. **B911**, 500 (2016).

[49] H. Zheng, L. F. Wei, H. Wen, and F. Y. Li, Electromagnetic response of gravitational waves passing through an alternating magnetic field: A scheme to probe high-frequency gravitational waves, Phys. Rev. D **98**, 064028 (2018).

[50] J. Liu, Q. Wang, L. Qin, B. Zhou, K. Wang, Y. Wang, L. Wang, Z. Zhang, Y. Dai, H. Liu, X. Hu, H. Wang, C. Cui, D. Wang, H. Wang, J. Sun, W. Sun, and L. Xiong, World record 32.35 tesla direct-current magnetic field generated with an all-superconducting magnet, Supercond. Sci. Technol. **33**, 03LT01 (2020).

[51] COMSOL MULTIPHYSICS v. 5.4., http://www.comsol.com.

[52] M. Jing, Y. Hu, J. Ma, H. Zhang, L. Zhang, L. Xiao, and S. Jia, Atomic superheterodyne receiver based on microwave-dressed Rydberg spectroscopy, Nat. Phys. **16**, 911 (2020).

[53] I. K. Kominis, T. W. Kornack, J. C. Allred, and M. V. Romalis, A subfemtotesla multichannel atomic magnetometer, Nature (London) **422**, 596 (2003).

[54] G. Arul Elango, G. Sudha, and B. Francis, Weak signal acquisition enhancement in software GPS receivers—prefiltering combined post-correlation detection approach, Appl. Comput. Inf. **13**, 66 (2017).

[55] R. H. Hadfield, Single-photon detectors for optical quantum information applications, Nat. Photonics **3**, 696 (2009).

[56] M. D. Eisaman, J. Fan, A. Migdall, and S. V. Polyakov, Invited review article: Single-photon sources and detectors, Rev. Sci. Instrum. **82**, 071101 (2011).

[57] Y. Liang and H. Zeng, Single-photon detection and its applications, Sci. China Mater. **57**, 1218 (2014).

[58] X. Li, L. Xie, and L. F. Wei, Atomic lenses and ideal single-photon detections, Phys. Rev. A **92**, 063840 (2015).

[59] W. Guo, X. Liu, Y. Wang, Q. Wei, L. F. Wei, J. Hubmayr, J. Fowler, J. Ullom, L. Vale, M. R. Vissers, and J. Gao, Counting near infrared photons with microwave kinetic inductance detectors, Appl. Phys. Lett. **110**, 212601 (2017).

[60] T. B. Propp and S. J. van Enk, Quantum networks for single photon detection, Phys. Rev. A **100**, 033836 (2019).

[61] E. Holdengreber, X. Gao, M. Mizrahi, S. E. Schacham, and E. Farber, Superior impedance matching of THz antennas with high temperature superconducting Josephson junctions, Supercond. Sci. Technol. **32**, 074006 (2019).

[62] T. H. Boyer, Derivation of the blackbody radiation spectrum without quantum assumptions, Phys. Rev. **182**, 1374 (1969).

[63] L. P. Grishchuk, *Relic Gravitational Waves and Their Detection* (Springer, Berlin, Heidelberg), pp. 167–192.

[64] L. P. Grishchuk, The implications of microwave background anisotropies for laser-interferometer-tested gravitational waves, Classical Quantum Gravity **14**, 1445 (1997).